Inorganic Chemistry

Article

pubs.acs.org/IC

Characterization of an Iron−Ruthenium Interaction in a Ferrocene Diamide Complex

Aaron G. Green,[†] Matthew D. Kiesz,[†] Jeremy V. Oria,[†] Andrew G. Elliott,[†] Andrew K. Buechler,[†] Johannes Hohenberger,[‡] Karsten Meyer,[‡] Jeffrey I. Zink,*[,†] and Paula L. Diaconescu*[,†]

[†]Department of Chemistry & Biochemistry, University of California, Los Angeles, California 90095, United States

[‡]Department of Chemistry and Pharmacy, Friedrich-Alexander-University Erlangen-Nürnberg, 91058 Erlangen, Germany

Supporting Information

ABSTRACT: Reaction of $[fc(NH_2)_2]RuCl_2(PPh_3)_2$ (fc = 1,1′-ferrocenylene) with 2 equiv of KO^{t}Bu led to the formation of a diamido ruthenium complex, $[fc(NH)_2]Ru(PPh_3)_2$, whose solid-state molecular structure revealed a short Fe−Ru distance. A metal-to-metal charge transfer band was observed in the electronic absorption spectrum of $[fc(NH)_2]Ru(PPh_3)_2$. The Fe−Ru interaction was characterized by resonance Raman spectroscopy for the first time and also by ^{1}H NMR, UV−vis, NIR, Mössbauer spectroscopy, and X-ray crystallography. Density functional theory (DFT) calculations including natural bond order analysis, Bader's atom in molecules method, and time-dependent DFT (TDDFT) provided further support that the iron−ruthenium bond is a weak donor−acceptor interaction with iron acting as the Lewis base.

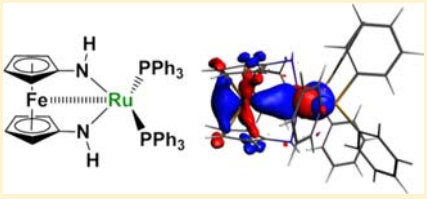

1. INTRODUCTION

Metal−metal bonds have been the subject of intense research and discussion.[1] Specifically, interactions between metal centers in bimetallic complexes can give rise to interesting electronic and magnetic properties[2−13] and novel reactivity.[14−20] Ferrocene derivatives[21] have seen widespread use as ancillary ligands for metal complexes,[21−24] largely because of the unique steric and electronic properties of the flexible and redox-active[25,26] ferrocene backbone. Metal complexes supported by chelating 1,1′-ferrocenediyl derivatives are particularly interesting and may allow a direct interaction between iron and the metal center.[27−29]

Weak interactions between the ferrocene iron with both early and late transition metals have been reported;[30−37] however, the nature of these interactions has been controversial. For example, the Seyferth group found that upon the oxidative addition of 1,2,3-trithia[3]ferrocene to $Pd(PPh_3)_4$, a four-coordinate palladium complex was formed, featuring an iron−palladium bond.[32] Sato and co-workers also synthesized a variety of late transition metal complexes that showed an interaction between the iron and the metal; that interaction was characterized by X-ray crystallography, NMR, and absorption spectroscopy.[38,39]

For group 4 metals, complexes supported by 1,1′-ferrocene diamide ligands were initially reported by Arnold et al., who showed that a highly reactive cationic titanium(IV) species was stabilized by an interaction with iron.[31] Recently, the Stephan group reported that ferrocene can stabilize cyclopentadienyl zirconium alkyl cations through an iron−zirconium interaction.[30] In both cases, the iron−metal interactions were established based on structural parameters obtained from X-ray crystallography.

Weak metal−metal bonding was reviewed by Braunschweig et al. from the perspective of Lewis pairs.[40] X-ray crystallography, Mössbauer, X-ray absorption spectroscopy, and computational methods were listed as methods used to determine the nature of weak metal−metal interactions. The authors also noted that it was especially difficult to assign the Lewis base and the Lewis acid in the case of 1,1′-ferrocenediyl (fc) complexes of middle-to-late transition metals. Such an assignment is important in expanding the concept of transition metal Lewis basicity, which is of fundamental interest in understanding the reactivity of the corresponding metal complexes.[40] This concept is difficult to grasp since most transition metals are viewed as Lewis acids. Herein, we report the characterization of $[fc(NH)_2]Ru(PPh_3)_2$ (fc = 1,1′-ferrocenylene),[41] a complex that features a short Fe−Ru distance, consistent with an iron−ruthenium donor−acceptor interaction. This interaction was characterized by electronic absorption, Mössbauer, and, for the first time, resonance Raman spectroscopy in conjunction with density functional theory (DFT) calculations. Resonance Raman studies were also carried out on previously published palladium complexes that feature an iron−palladium interaction to validate the method. Aside from the importance of understanding the role played by the Lewis basicity of metal ions in organic reactions (for example, oxidative addition processes),[40] the present article shows that it is possible to characterize donor−acceptor interactions between two metals with similar Lewis acid/base character, even when these properties are dependent on their chemical environment.

Received: March 28, 2013
Published: April 19, 2013

2. RESULTS AND DISCUSSION

Synthesis and Structural Characterization. We have been interested in the chemistry of substituted 1,1′-ferrocene diamides as ancillary ligands for group 3 metals, lanthanides, and uranium.[27,28] In some instances, we observed short iron−metal distances and proposed that the ferrocene diamide supporting ligand was instrumental in stabilizing certain bonding motifs.[42,43] To differentiate between the influence of the nitrogen substituent and that of the ferrocene diamide core, we chose the parent 1,1′-ferrocene diamine, $(fc(NH_2)_2)$, as a platform to study metal−metal bonding. Inspired by Seyferth's and Sato's pioneering work with late transition metals, and because of numerous reports of stable amine[44−50] and amide[50−53] ruthenium compounds, we chose to investigate ruthenium complexes. Additionally, the syntheses of the dichloride $[fc(NH_2)_2]RuCl_2(PPh_3)_2$ (**1**) and of the diamide $[fc(NH)_2]Ru(PPh_3)_2$ (**2**) species were recently reported by us.[41]

Compound **2** was prepared by the reaction of **1** with KO^{t}Bu (Scheme 1).[41] Interestingly, **2** was found to be remarkably

Scheme 1. Syntheses of Complexes 1−4

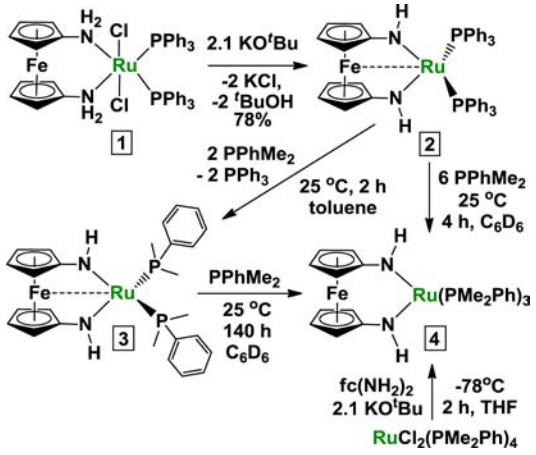

resistant to σ donors. No reactions were observed in the presence of tetrahydrofuran (THF), MeCN, or aniline. When 2 equiv of PMe_2Ph were added to **2**, however, a new bisphosphine complex $[fc(NH)_2]Ru(PMe_2Ph)_2$, **3**, was formed (Scheme 1). This complex was isolated as black crystals, which decomposed slowly at room temperature in the absence of PMe_2Ph to form 1,1′-ferrocene diamine. Addition of a third equivalent of phosphine to this complex resulted in the formation of the trisphosphine species $[fc(NH)_2]Ru(PMe_2Ph)_3$, **4**, as determined by ^{1}H and ^{31}P NMR spectroscopy. The formation of **4** could also be observed by the direct addition of 6 equiv of $PPhMe_2$ to **2**, or by the addition of 1 equiv of $fc(NH_2)_2$ to $RuCl_2(PPhMe_2)_4$[54] at −78 °C followed by the addition of 2.1 equiv of KO^{t}Bu (see the Supporting Information for details). Compound **4** could not be isolated since it rapidly decomposed to form $fc(NH_2)_2$ and an intractable mixture containing phosphorus species.

Compounds **1**, **2**, and **3** were characterized by X-ray crystallography. The solid-state molecular structure of **1** (Figure 1) exhibits a distorted octahedral ruthenium complex with chloride ligands in the axial positions and a Cl−Ru−Cl angle of 165°. The Ru−N distances were 2.24 Å and 2.27 Å, while the Ru−P distances were 2.31 Å and 2.32 Å. In addition, the Cp-

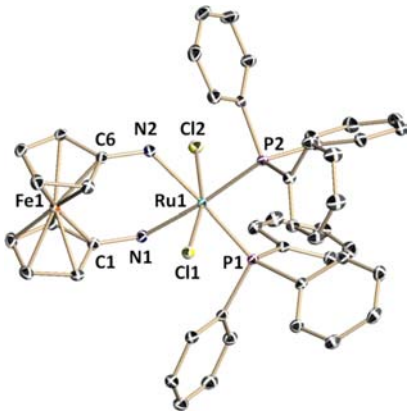

Figure 1. Thermal-ellipsoid (50% probability) representation of **1**. Hydrogen atoms were omitted for clarity. Selected distances [Å] and angles [deg]: Ru1−Cl1 2.3948(5), Ru1−Cl2 2.4427(4), Ru1−P1 2.3150(5), Ru1−P2 2.3205(4), Ru1−N1 2.2669(11), Ru1−N2 2.2407(12); Cl1−Ru1−Cl2 164.96(1), Cl1−Ru1−P1 91.71(1), Cl1−Ru1−P2 93.60(2), Cl1−Ru1−N1 92.36(3), Cl1−Ru1−N2 89.36(3), Cl2−Ru1−P1 100.57(1), Cl2−Ru1−P2 93.91(2), Cl2−Ru1−N1 79.43(3), Cl2−Ru1−N2 77.69(3), P1−Ru1−P2 95.13(1), P1−Ru1−N1 88.51(3), P1−Ru1−N2 175.04(3), P2−Ru1−N1 172.93(3), P2−Ru1−N2 89.64(3), N1−Ru1−N2 86.61(4), Fe1−C1−N1 127.48(8), Fe1−C6−N2 126.78(9), twist 1.66, tilt 102.90.

ring twist angle was 1.7° and the Cp-Cp tilt angle was 102.9° (see Figure 2 for an explanation of twist and tilt).

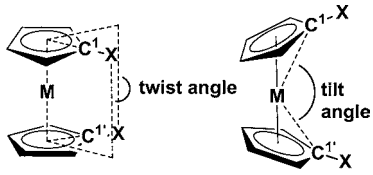

Figure 2. Description of twist and tilt angle for 1,1′-ferrocenediyl ligands. Twist angles were calculated by measuring the angle between the two planes formed by C^1 and the centroids of the two Cp rings, and $C^{1'}$ and the centroids of the two Cp rings. The Cp tilt angle is C^1−Fe-$C^{1'}$; the Cp-Cp tilt angle in ferrocene is 107.4°.

The X-ray crystal structure of **2** (Figure 3) shows the ruthenium center in a distorted trigonal bipyramidal geometry with an N1−Ru−N2 angle of 159° and a Ru−N distance of 2.16 Å. The Ru−P distances decreased to 2.20 Å. More importantly, a drastic decrease in the iron−ruthenium distance in **2** (2.80 Å) compared to **1** (4.20 Å) was observed. The Fe−Ru distance in **2** is only 0.02 Å greater than the sum of the covalent radii (2.78 Å),[55] indicating that a metal−metal interaction may be present. The Cp-ring twist angle was 10.61° and the Cp-Cp tilt angle was 121.63° (for comparison, the Cp-Cp tilt angle in ferrocene is 107.4°) indicating appreciable distortion of the ferrocene ligand relative to **1**. The solid-state molecular structure of **3** (Figure 4) exhibits similar features to complex **2** with a notably short Fe−Ru distance of 2.77 Å, a Cp-ring twist angle of 0.1° and a Cp-Cp tilt angle of 118.7°.

The ^{1}H NMR spectra of **2** and **3** in C_6D_6 exhibit a large splitting between the signals for the α (4.10 and 4.21 ppm, respectively) and β (2.20 and 2.08 ppm, respectively) Cp protons ($\Delta\delta$ = 1.9 and 2.1 ppm, respectively). Splitting of the α and β proton peaks of the Cp rings has been previously explained by the anisotropic effect of the iron−metal bond

dx.doi.org/10.1021/ic400773s | Inorg. Chem. 2013, 52, 5603−5610

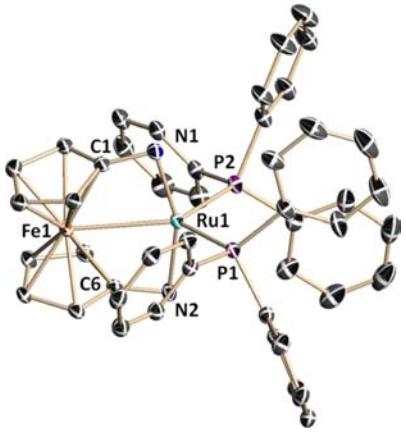

Figure 3. Thermal-ellipsoid (50% probability) representation of one of the two crystallographically independent molecules of **2**. Hydrogen atoms were omitted for clarity. Selected distances [Å] and angles [deg]: Ru1−Fe1 2.7994(5), Ru1−P1 2.2033(7), Ru1−P2 2.2026(7), Ru1−N1 2.1586(22), Ru1−N2 2.1596(22); Fe1−Ru1−P1 130.02(2), Fe1−Ru1−P2 131.61(2), Fe1−Ru1−N1 79.67(6), Fe1−Ru1−N2 79.70(6), P1−Ru1−P2 98.37(3), P1−Ru1−N1 93.63(7), P1−Ru1−N2 100.06(7), P2−Ru1−N1 99.56(7), P2−Ru1−N2 93.67(7), N1−Ru1−N2 159.36(9), Cp-Fe1-Cp 170.2, twist 10.31, tilt 121.63.

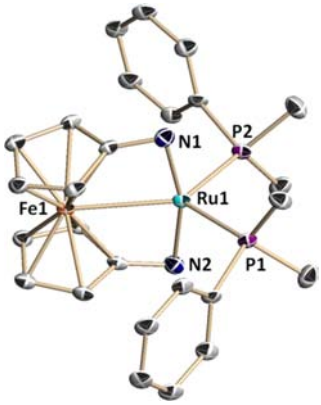

Figure 4. Thermal-ellipsoid (50% probability) representation of **3**. Hydrogen atoms were omitted for clarity. Selected distances [Å] and angles [deg]: Ru1−Fe1 2.768(2), Ru1−P1 2.192(1), Ru1−N1 2.163(4); Fe1−Ru1−P1 133.40(3), Fe1−Ru1−N1 82.20(10), P1−Ru1−P2 93.20(6), P1−Ru1−N1 93.07(11), N1−Ru1−N1 164.39(20), Ru1−N1−C9 87.75(26), Cp-Fe1-Cp 173.09, twist 0.06, tilt 118.71.

providing a shielding effect on the α protons, while the β protons are less affected because they are further away.[35−39]

Mössbauer Spectroscopy. To probe the electronic structure of iron in complexes **1** and **2**, Mössbauer spectroscopy studies were carried out. The Mössbauer spectrum of **1** (Figure 5) exhibits a doublet at 0.53(1) mm s^{-1}, consistent with an Fe(II) center. The Mössbauer spectrum obtained for **2** (Figure 5) also exhibits a doublet, at δ = 0.56(1), indicating an Fe(II) center. For comparison, Mössbauer spectroscopic studies were also carried out (Figure 5) on [(dppf)Pd(PPh_3)][BF_4]$_2$ (dppf = 1,1′-bis(diphenylphosphino)ferrocene), **5**, and [(dppf)Pd(4-picoline)$_2$][BF_4]$_2$, **6**.[39] These measurements resulted in data that are consistent with Fe(II) centers. The results obtained for **1**, **2**, **5**, and **6** are expected since the ^{1}H NMR spectra for these complexes exhibit diamagnetic characteristics.

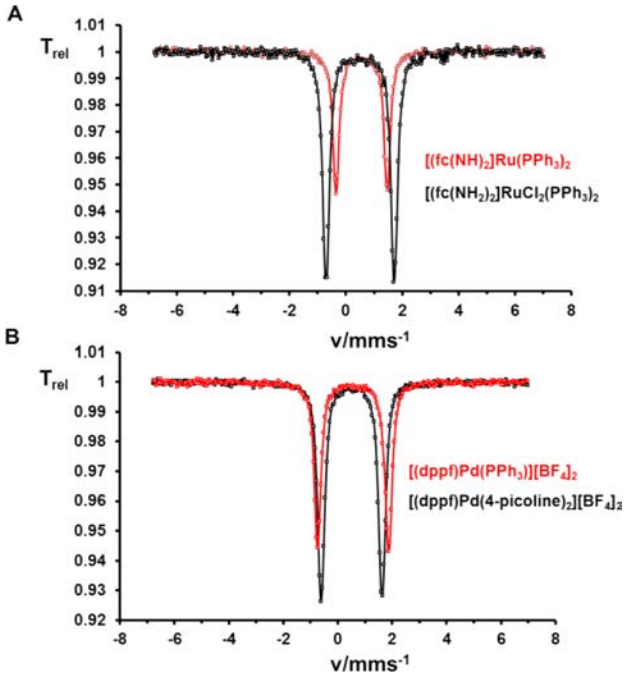

Figure 5. (A) Overlaid Mössbauer spectra of **1** and **2**. (B) Overlaid Mössbauer spectra of **5** and **6**.

DFT Calculations. DFT geometry optimizations were carried out with ADF2012.01 on the full molecules of **1**, **2**, and **3**. For **2**, calculations were performed at the LDA[64] and PW91[65] theory levels, with full electron (no frozen cores) triple-ζ-potential (TZP) basis sets, and using the relativistic scalar ZORA approximation. The values for the calculated Fe−Ru distance in **2**, 2.76 Å (LDA) and 2.87 Å (PW91, see the Supporting Information for other parameters), match well the experimental distance determined by X-ray crystallography (2.80 Å, see above). In accord with the short Fe−Ru distance, HOMO-6 of **2** shows a σ interaction between the two metals (Figure 6). The calculated Mayer bond order[69,70] for the iron−ruthenium interaction for **2** and **3** is 0.28 (PW91) and 0.26, respectively. For comparison, the Mayer bond orders for the single Ru−Ru bond in [$Ru(CO)_4$]$_8$ and $Ru_3(CO)_{12}$ were found to be 0.70 and 0.62, respectively,[71] indicating that the Fe−Ru bonds of **2** and **3** are weaker than metal−metal single bonds.

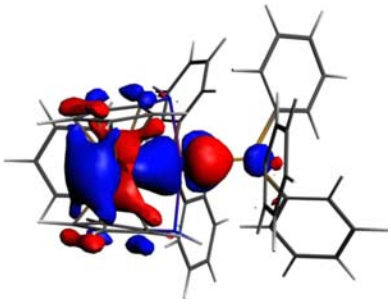

Figure 6. HOMO-6 for **2**. Orbitals are similar for the LDA and PW91 calculations.

The optimized coordinates were used for further analysis with NBO 5.0[66] and Bader's atoms in molecules (AIM) methods.[67,68] Analysis of the generated natural bond orbitals (NBOs) shows overlap from two occupied valence orbitals

dx.doi.org/10.1021/ic400773s | Inorg. Chem. 2013, 52, 5603−5610

centered on Fe and Ru (Figure 7). Natural localized molecular orbitals (NLMOs) generated from these NBOs show a

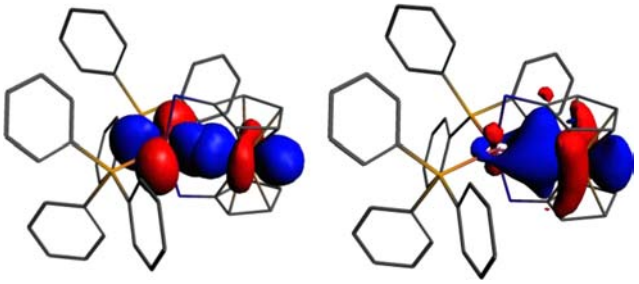

Figure 7. Left: Overlap between NBOs 209 (Ru) and 211 (Fe), right: NLMO 211 for **2**.

significant contribution from Fe and a small total (7.15%) contribution from Ru (Figure 7 and Supporting Information, Figure S8). Conversely, three NLMOs centered on Ru only have a 0.39% contribution from Fe (see the Supporting Information for details). These data indicate that there is donation from iron to ruthenium. Natural population analysis shows that there is a net linear overlap of 0.29 (both LDA and PW91 calculations gave the same value) between the metal centers.

Additionally, an NBO second order perturbation theory analysis of the donor–acceptor data shows stabilizing interactions (10.1 kcal/mol total energy) from occupied valence orbitals on iron to empty orbitals on ruthenium. The reverse, that is, stabilizing interactions from occupied valence orbitals on ruthenium to empty orbitals on iron, was not found, consistent with a donor–acceptor interaction between iron and ruthenium with iron functioning as the donor.

Topological analysis of electron density was carried out using Bader's atoms in molecule (AIM) theory. This module is provided as a subroutine in ADF2012. AIM identifies any type of bond by calculating a (3, −1) critical point, and it differentiates between covalent bonds, on one hand, and weak interactions such as hydrogen bonds, van der Waals, and donor–acceptor, on the other, by the value of the Laplacian (∇^2_ρ). If $\nabla^2_\rho < 0$, the interaction is considered covalent. If $\nabla^2_\rho > 0$, the interaction is a weak interaction. AIM has been used to calculate bond critical points between two metal centers[72] and in ferrocene complexes.[73] A (3, −1) critical point was found in **2** at 1.43 Å (PW91), the midpoint of the Fe–Ru distance, supporting the presence of a weak interaction between the two metal centers. Calculation of the Laplacian for **2** shows greater electron density surrounding iron than ruthenium, consistent with the NBO findings of electron donation from iron to ruthenium. The contour plot of the Laplacian in the plane of iron, ruthenium, and one of the amide nitrogen atoms (Figure 8) shows low electron density between the two metal centers, with the gradient consistent with a weak interaction. For comparison, a significant gradient is found between the amide nitrogens and carbons, indicative of a covalent bond. Combined with the short distances determined experimentally and the spectroscopic data discussed above, the results of DFT calculations support the existence of a weak interaction between iron and ruthenium in **2**, consistent with electron donation from iron to ruthenium.

Electronic Absorption Spectroscopy. The UV–vis and NIR (near-infrared) spectra of **1** and **2** (Figure 9 and Supporting Information) show remarkable differences. The

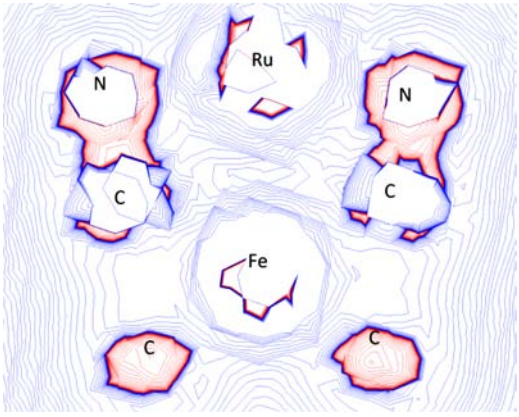

Figure 8. Contour plot of the Laplacian ∇^2_ρ in the plane of iron, ruthenium, and one of the amide nitrogen atoms for **2**. Red lines indicate areas of high charge $\nabla^2_\rho < 0$, blue lines indicate depletion of charge $\nabla^2_\rho > 0$.

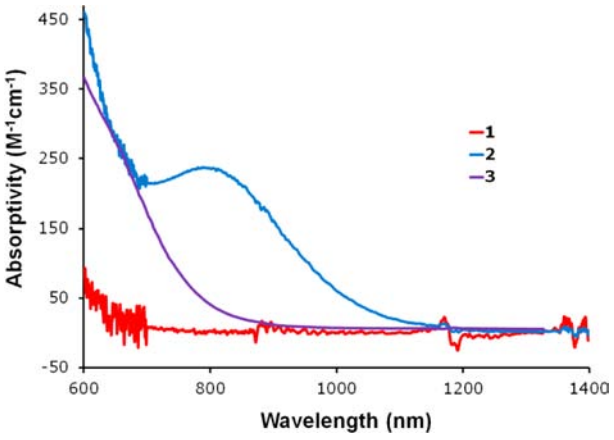

Figure 9. Near-infrared spectra in THF of **1** (2.5 mM), **2** (0.8 mM), and **3** (0.8 mM).

dichloride complex exhibits peaks at 320 nm (ε = 5784 M^{-1} cm^{-1}) and 500 nm (ε = 578 M^{-1} cm^{-1}), which were assigned to Fe-Cp charge transfer and Fe d-d transitions. Similarly, the diamide complexes **2** and **3** (Figure 9) exhibit peaks at 360 (ε = 9647 M^{-1} cm^{-1}) and 352 (ε = 6258 M^{-1} cm^{-1}) nm, 530 (ε = 1214 M^{-1} cm^{-1}) and 454 (ε = 1427 M^{-1} cm^{-1}) nm. In addition to those peaks, an absorption at 798 (ε = 236 M^{-1} cm^{-1}) and 663 (ε = 261 M^{-1} cm^{-1}) nm, respectively, is observed for these two complexes. As for **1**, the first two peaks in the UV–vis spectra of **2** and **3** were assigned to Fe-Cp and d-d transitions (see also the Supporting Information for calculated transitions). By comparison to Sato's previous observations, the third, weakly absorbing peak, was assigned to an iron–ruthenium charge transfer band.[39] The increase in energy of the iron–ruthenium charge transfer band from **2** to **3** can be expected since PMe_2Ph is a stronger σ-donor than PPh_3.

The time-dependent DFT calculated excitation spectrum of **2** matches the UV–vis and NIR spectra obtained experimentally, with an offset of −350 nm (see the Supporting Information for details). These calculations show a low energy transition corresponding to the IVCT band, calculated at 768 nm (corresponding to the 798 nm absorption found experimentally); this transition arises from promoting an electron from the highest occupied molecular orbital (HOMO) to the lowest unoccupied molecular orbital

dx.doi.org/10.1021/ic400773s | Inorg. Chem. 2013, 52, 5603–5610

(LUMO). The HOMO of **2** (Figure 10) was found to consist (see the Supporting Information for details) of mainly

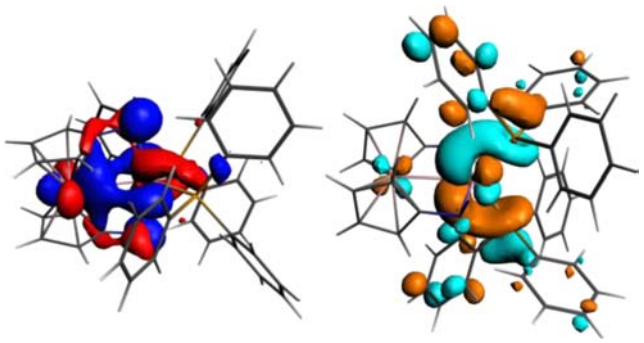

Figure 10. HOMO (left) and LUMO (right) of **2** (isosurface value = 0.03).

ruthenium d orbitals (31% total contribution) and iron d orbitals (22% total contribution) in addition to contributions from nitrogen p orbitals (19% total contribution). In contrast, the LUMO of **2** (Figure 10) is primarily ruthenium based with some contribution from the phosphorus atoms (see the Supporting Information for details). Neither molecular orbital shows contributions from the phosphine ligands or the ferrocene Cp rings. The HOMO shows antibonding interactions between the ruthenium and the nitrogen, with a nonbonding interaction between the ruthenium and iron. The LUMO shows no contribution from the nitrogen, with an antibonding interaction between ruthenium and iron; this indicates that promotion of an electron from HOMO to LUMO weakens the Ru–Fe bond while strengthening the Ru–N bond. Therefore, the change in bond length of the iron–ruthenium interaction may be probed by resonance Raman spectroscopy (see below).

Resonance Raman Spectroscopy. Resonance Raman spectroscopy utilizes photons that are in resonance with an electronic transition of interest. When an electronic transition occurs, the electron density of the molecule shifts relative to the ground state. Normal modes with nuclear motion corresponding to the changes in electron density in the excited state are displaced relative to the ground state, enhancing the Raman signal. Symmetric transitions are resonantly enhanced most strongly because the slope of the excited state potential energy surface is nonzero at the Franck–Condon region; the intensity of scattering scales with the square of the distortion.[56,57] The ability to amplify the intensity of vibrations when in resonance with an electronic transition enables resonance Raman spectroscopy to assist in the assignment of these specific electronic transitions.[57] This technique,[58,59] as well as regular Raman spectroscopy,[60,61] has been used previously to establish electronic communication within bimetallic complexes. However, the present study represents the first instance when resonance Raman spectroscopy is used to investigate the nature of weak metal–metal interactions. Here we will demonstrate the resonance enhancement of a Raman active iron–metal (Pd or Ru) stretch when in resonance with the charge transfer electronic transition (Figure 11). This resonance enhancement, in conjunction with the results of DFT calculations, supports the assignment of weak metal–metal interactions.

To validate this method, we first undertook resonance Raman spectroscopy studies on the pair of previously reported complexes, $[(dppf)Pd(PPh_3)][BF_4]_2$ (dppf = 1,1′-bis-

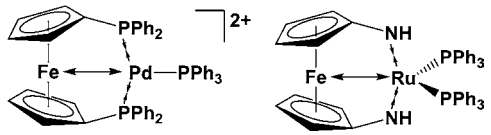

Figure 11. Displacement vectors for the normal metal–metal stretching mode of **5** (left) and **2** (right). Displacement involves primarily elongation along the metal–metal axis and contraction along the Pd–P or Ru–N axis.

(diphenylphosphino)ferrocene), **5**, which exhibits metal-to-metal charge transfer, and $[(dppf)Pd(4\text{-picoline})_2][BF_4]_2$, **6**, which does not.[39] As expected, **5** showed enhancement of a vibration at 330 cm^{-1} with displacement along the iron–palladium axis as the excitation wavelength passed the metal-to-metal charge transfer (Figure 12). In contrast, **6** showed no

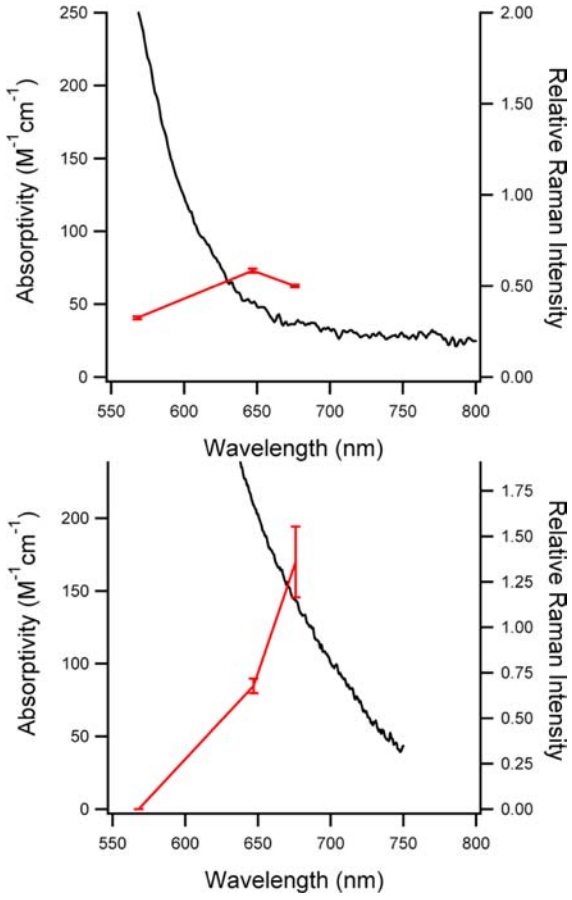

Figure 12. Raman intensity for 347 cm^{-1} mode of **6** (top) and 330 cm^{-1} mode of **5** (bottom) as a function of excitation wavelength superimposed with absorption spectra. Raman intensities for both compounds are scaled relative to 750 cm^{-1} vibration of PF_6^- (internal standard). Intensities are calculated by fitting vibrations with Gaussian functions. Error bars are derived from the error in fitting.

significant vibrational enhancement upon red excitation (Figure 12). Other vibrations of **6** displayed a similar trend of lowered relative intensity at 568 nm. That loss was attributed to Raman de-enhancement and was only observed at 568 nm for **6** because of the red shift of the Fe d-d transitions.

The Raman spectra of **1** and **2** were obtained at excitation wavelengths of 407, 476, 530, 568, 647, and 676 nm (Figure 13, see the Supporting Information for all spectra), using a Kr^+ ion

dx.doi.org/10.1021/ic400773s | Inorg. Chem. 2013, 52, 5603–5610

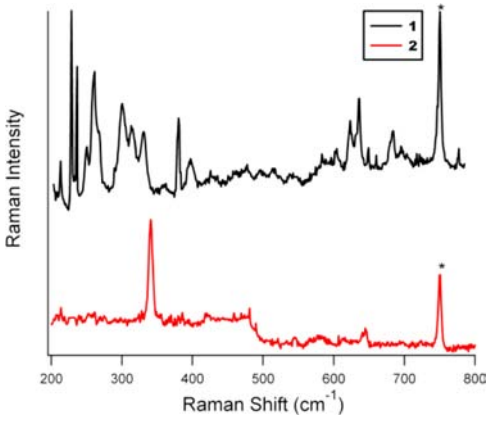

Figure 13. Raman spectra of **1** and **2** upon 676.4 nm excitation. Asterisks indicate the vibration (715 cm^{-1}) of the internal standard, KNO_3.

laser. As expected, the Raman spectra for **1** showed no trend of enhancement in any of the vibrational modes as the excitation wavelength increased (Figure 14). In the case of **2**, however, significant enhancement of the 342 cm^{-1} mode was observed as the excitation wavelength of the laser was increased (Figure 14). Examination of the resonance Raman spectra of **1** and **2** upon higher excitation energies reveals de-enhancement trends typical of cyclopentadienyl sandwich compounds.[62,63]

The vibrational modes that appear in the resonance Raman spectra were assigned using DFT calculations at the PW91/TZP level. The vibration at 342 cm^{-1} was assigned to a normal mode consisting primarily of an iron−ruthenium stretch in conjunction with nitrogen−ruthenium stretches similar to the normal mode previously described for **5**; as the iron−ruthenium distance expands the nitrogen−ruthenium bond contracts. The calculated frequency for this vibration is 256 cm^{-1}.

Additionally, the changes in electron density between the HOMO and LUMO (Figure 10) support this assignment. Because the 798 nm absorption is assigned to the HOMO to LUMO transition, normal modes with displacement coincident with the changes in electron density will be enhanced in the resonance Raman spectrum. Specifically, the NIR metal-to-metal charge transfer weakens the iron−ruthenium bond, thereby elongating it and producing a stretch along the metal−metal axis. In addition to the increase of the Ru−Fe distance, this mode shows contraction of the Ru−N bonds. The resonance enhancement of this mode increases as the excitation wavelength nears the maximum of the charge transfer band. Thus, the change in the Ru−Fe distance results primarily from the interaction of the two metal centers.

3. CONCLUSIONS

In summary, a weak, donor−acceptor interaction between iron and ruthenium in complexes **2** and **3** was described. This interaction was characterized by ^1H NMR, UV−vis, NIR, Mössbauer, and Raman spectroscopy, X-ray crystallography, and DFT calculations. The Raman spectra of **2** and **5** exhibit similar features indicating that resonance Raman spectroscopy, in conjunction with UV−vis/NIR spectroscopy, is a useful tool for determining whether or not a weak interaction between two metal centers exists in such complexes. Furthermore, DFT calculations indicate that the metal−metal interaction is primarily an Fe−Ru donor−acceptor interaction with iron

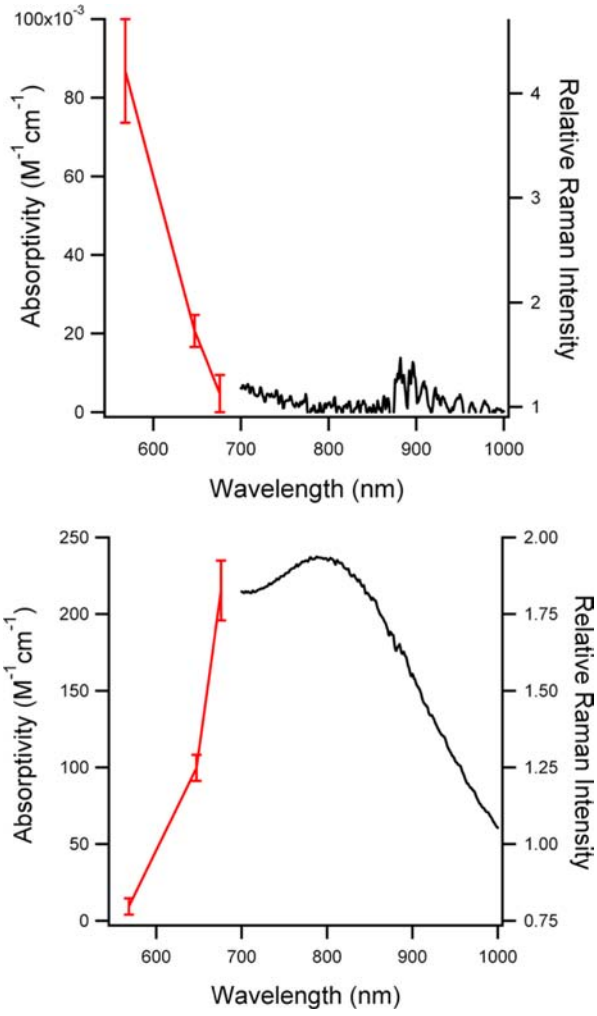

Figure 14. Raman intensity for 300 cm^{-1} mode of **1** (top) and 342 cm^{-1} mode of **2** (bottom) as a function of excitation wavelength superimposed with the corresponding NIR spectrum. Raman intensities for both compounds are scaled relative to 750 cm^{-1} vibration of PF_6^- (internal standard). Intensities are calculated by fitting vibrations with Gaussian functions. Error bars are derived from the error in fitting.

acting as the Lewis base. The present work shows that an in-depth, combined spectroscopic and computational study is powerful in investigating weak metal−metal interactions with complexes **2**, **3**, and **5** representing well characterized examples.

■ ASSOCIATED CONTENT

Ⓢ Supporting Information

X-ray crystallographic data in CIF format for complexes **1**, **2**, and **3**, spectroscopic and DFT data. This material is available free of charge via the Internet at http://pubs.acs.org.

■ AUTHOR INFORMATION

Corresponding Author

*E-mail: zink@chem.ucla.edu (J.I.Z.), pld@chem.ucla.edu (P.L.D.).

Notes

The authors declare no competing financial interest.

■ ACKNOWLEDGMENTS

This material is based upon work supported by the National Science Foundation (CAREER Grant to P.L.D. and Graduate Research Fellowship DGE-0707424 to A.G.G.), Sloan Foundation, University of Erlangen Nürnberg, DFG, and the Bavarian California Technology Center (BaCaTec).

■ REFERENCES

(1) *Structure and Bonding: Metal-Metal Bonding*; Springer-Verlag: Berlin, Germany, 2010.
(2) Barlow, S.; O'Hare, D. *Chem. Rev.* **1997**, *97*, 637.
(3) Samoc, M.; Gauthier, N.; Cifuentes, M. P.; Paul, F.; Lapinte, C.; Humphrey, M. G. *Angew. Chem., Int. Ed.* **2006**, *45*, 7376.
(4) Mueller-Westerhoff, U. T.; Eilbracht, P. *J. Am. Chem. Soc.* **1972**, *94*, 9272.
(5) Aguirre-Etcheverry, P.; O'Hare, D. *Chem. Rev.* **2010**, *110*, 4839.
(6) Tsurugi, H.; Nagae, H.; Mashima, K. *Chem. Commun.* **2011**, *47*, 5620.
(7) Matsuo, Y.; Tahara, K.; Fujita, T.; Nakamura, E. *Angew. Chem., Int. Ed.* **2009**, *48*, 6239.
(8) Figueira-Duarte, T. M.; Lloveras, V.; Vidal-Gancedo, J.; Gegout, A.; Delavaux-Nicot, B.; Welter, R.; Veciana, J.; Rovira, C.; Nierengarten, J.-F. *Chem. Commun.* **2007**, 4345.
(9) Sun, H.; Steeb, J.; Kaifer, A. E. *J. Am. Chem. Soc.* **2006**, *128*, 2820.
(10) Kaim, W.; Lahiri, G. K. *Angew. Chem., Int. Ed.* **2007**, *46*, 1778.
(11) Sixt, T.; Sieger, M.; Krafft, M. J.; Bubrin, D.; Fiedler, J.; Kaim, W. *Organometallics* **2010**, *29*, 5511.
(12) Poneti, G.; Mannini, M.; Sorace, L.; Sainctavit, P.; Arrio, M.-A.; Otero, E.; Criginski Cezar, J.; Dei, A. *Angew. Chem., Int. Ed.* **2010**, *49*, 1954.
(13) Hilfiger, M. G.; Chen, M.; Brinzari, T. V.; Nocera, T. M.; Shatruk, M.; Petasis, D. T.; Musfeldt, J. L.; Achim, C.; Dunbar, K. R. *Angew. Chem., Int. Ed.* **2010**, *49*, 1410.
(14) Allgeier, A. M.; Mirkin, C. A. *Angew. Chem., Int. Ed.* **1998**, *37*, 894.
(15) Yoon, H. J.; Kuwabara, J.; Kim, J.-H.; Mirkin, C. A. *Science* **2010**, *330*, 66.
(16) Gusev, O. V.; Peganova, T. A.; Kalsin, A. M.; Vologdin, N. V.; Petrovskii, P. V.; Lyssenko, K. A.; Tsvetkov, A. V.; Beletskaya, I. P. *Organometallics* **2006**, *25*, 2750.
(17) Bianchini, C.; Meli, A.; Oberhauser, W.; Parisel, S.; Passaglia, E.; Ciardelli, F.; Gusev, O. V.; Kal'sin, A. M.; Vologdin, N. V. *Organometallics* **2005**, *24*, 1018.
(18) Gusev, O. V.; Kalsin, A. M.; Petrovskii, P. V.; Lyssenko, K. A.; Oprunenko, Y. F.; Bianchini, C.; Meli, A.; Oberhauser, W. *Organometallics* **2003**, *22*, 913.
(19) Lorkovic, I. M.; Duff, R. R.; Wrighton, M. S. *J. Am. Chem. Soc.* **1995**, *117*, 3617.
(20) Lorkovic, I. M.; Wrighton, M. S.; Davis, W. M. *J. Am. Chem. Soc.* **1994**, *116*, 6220.
(21) Togni, A.; Hayashi, T. *Ferrocenes: homogeneous catalysis, organic synthesis, materials science*; VCH Publishers: Weinheim, Germany, 1995.
(22) Siemeling, U.; Auch, T.-C. *Chem. Soc. Rev.* **2005**, *34*, 584.
(23) Siemeling, U. *Z. Anorg. Chem.* **2005**, *631*, 2957.
(24) Atkinson, R. C. J.; Gibson, V. C.; Long, N. J. *Chem. Soc. Rev.* **2004**, *33*, 313.
(25) Connelly, N. G.; Geiger, W. E. *Chem. Rev.* **1996**, *96*, 877.
(26) Astruc, D. *New J. Chem.* **2009**, *33*, 1191.
(27) Diaconescu, P. L. *Comments Inorg. Chem.* **2010**, *31*, 196.
(28) Diaconescu, P. L. *Acc. Chem. Res.* **2010**, *43*, 1352.
(29) van Leeuwen, P. W. N. M.; Zuideveld, M. A.; Swennenhuis, B. H. G.; Freixa, Z.; Kamer, P. C. J.; Goubitz, K.; Fraanje, J.; Lutz, M.; Spek, A. L. *J. Am. Chem. Soc.* **2003**, *125*, 5523.
(30) Ramos, A.; Otten, E.; Stephan, D. W. *J. Am. Chem. Soc.* **2009**, *131*, 15610.
(31) Shafir, A.; Arnold, J. *J. Am. Chem. Soc.* **2001**, *123*, 9212.
(32) Seyferth, D.; Hames, B. W.; Rucker, T. G.; Cowie, M.; Dickson, R. S. *Organometallics* **1983**, *2*, 472.
(33) Mann, G.; Shelby, Q.; Roy, A. H.; Hartwig, J. F. *Organometallics* **2003**, *22*, 2775.
(34) Metallinos, C.; Tremblay, D.; Barrett, F. B.; Taylor, N. J. *J. Organomet. Chem.* **2006**, *691*, 2044.
(35) Akabori, S.; Kumagai, T.; Shirahige, T.; Sato, S.; Kawazoe, K.; Tamura, C.; Sato, M. *Organometallics* **1987**, *6*, 526.
(36) Akabori, S.; Kumagai, T.; Shirahige, T.; Sato, S.; Kawazoe, K.; Tamura, C.; Sato, M. *Organometallics* **1987**, *6*, 2105.
(37) Sato, M.; Suzuki, K.; Asano, H.; Sekino, M.; Kawata, Y.; Habata, Y.; Akabori, S. *J. Organomet. Chem.* **1994**, *470*, 263.
(38) Sato, M.; Shigeta, H.; Sekino, M.; Akabori, S. *J. Organomet. Chem.* **1993**, *458*, 199.
(39) Sato, M.; Sekino, M.; Akabori, S. *J. Organomet. Chem.* **1988**, *344*, C31.
(40) Bauer, J.; Braunschweig, H.; Dewhurst, R. D. *Chem. Rev.* **2012**, *112*, 4329.
(41) Elliott, A. G.; Green, A. G.; Diaconescu, P. L. *Dalton Trans.* **2012**, *41*, 7852.
(42) Huang, W.; Khan, S. I.; Diaconescu, P. L. *J. Am. Chem. Soc.* **2011**, *133*, 10410.
(43) Huang, W.; Diaconescu, P. L. *Chem. Commun.* **2012**, *48*, 2216.
(44) Ford, P. C. *Coord. Chem. Rev.* **1970**, *5*, 75.
(45) Tfouni, E. *Coord. Chem. Rev.* **2000**, *196*, 281.
(46) Clapham, S. E.; Hadzovic, A.; Morris, R. H. *Coord. Chem. Rev.* **2004**, *248*, 2201.
(47) Ohkuma, T.; Koizumi, M.; Muñiz, K.; Hilt, G.; Kabuto, C.; Noyori, R. *J. Am. Chem. Soc.* **2002**, *124*, 6508.
(48) Ohkuma, T.; Ooka, H.; Hashiguchi, S.; Ikariya, T.; Noyori, R. *J. Am. Chem. Soc.* **1995**, *117*, 2675.
(49) Noyori, R.; Ohkuma, T. *Angew. Chem., Int. Ed.* **2001**, *40*, 40.
(50) Abdur-Rashid, K.; Clapham, S. E.; Hadzovic, A.; Harvey, J. N.; Lough, A. J.; Morris, R. H. *J. Am. Chem. Soc.* **2002**, *124*, 15104.
(51) Yi, C. S. *J. Organomet. Chem.* **2011**, *696*, 76.
(52) Gunnoe, T. B. *Eur. J. Inorg. Chem.* **2007**, *2007*, 1185.
(53) Bryndza, H. E.; Tam, W. *Chem. Rev.* **1988**, *88*, 1163.
(54) Armit, P. W.; Stephenson, t.A. *J. Organomet. Chem.* **1973**, *57*, C80.
(55) Cordero, B.; Gomez, V.; Platero-Prats, A. E.; Reves, M.; Echeverria, J.; Cremades, E.; Barragan, F.; Alvarez, S. *Dalton Trans.* **2008**, 2832.
(56) Heller, E. J.; Sundberg, R.; Tannor, D. *J. Phys. Chem.* **1982**, *86*, 1822.
(57) Shin, K. S. K.; Zink, J. I. *Inorg. Chem.* **1989**, *28*, 4358.
(58) Dallinger, R. F.; Miskowski, V. M.; Gray, H. B.; Woodruff, W. H. *J. Am. Chem. Soc.* **1981**, *103*, 1595.
(59) Shin, K. S.; Clark, R. J. H.; Zink, J. I. *J. Am. Chem. Soc.* **1989**, *111*, 4244.
(60) Curley, J. J.; Bergman, R. G.; Tilley, T. D. *Dalton Trans.* **2012**, *41*, 192.
(61) Schätzlein, A.; Schubart, M.; Findeis, B.; Gade, L. H.; Fickert, C.; Pikl, R.; Kiefer, W. *J. Mol. Struct.* **1997**, *408*−*409*, 373.
(62) Andrade, G. F. S.; Siqueira, L. J. A.; Ribeiro, M. C. C.; Sala, O.; Temperini, M. L. A. *J. Raman Spectrosc.* **2006**, *37*, 498.
(63) Bailey, S. E.; Cohan, J. S.; Zink, J. I. *J. Phys. Chem. B* **2000**, *104*, 10743.
(64) Ceperley, D. M.; Alder, B. J. *Phys. Rev. Lett.* **1980**, *45*, 566.
(65) Perdew, J. P.; Wang, Y. *Phys. Rev. B* **1992**, *45*, 13244.
(66) Glendening, E. D.; Badenhoop, J. K.; Reed, A. E.; Carpenter, J. E.; Bohmann, J. A.; Morales, C. M.; Weinhold, F. *NBO. Version 5.0*; Theoretical Chemistry Institute, University of Wisconsin: Madison, WI, 2001.
(67) Bader, R. F. W. *Atoms in Molecules - A Quantum Theory*; Oxford University Press: Oxford, U.K., 1990.
(68) Rodríguez, J. I.; Bader, R. F. W.; Ayers, P. W.; Michel, C.; Götz, A. W.; Bo, C. *Chem. Phys. Lett.* **2009**, *472*, 149.
(69) Mayer, I. *Chem. Phys. Lett.* **1983**, *97*, 270.

(70) Bridgeman, A. J.; Cavigliasso, G.; Ireland, L. R.; Rothery, J. *J. Chem. Soc., Dalton Trans.* **2001**, 2095.
(71) Niskanen, M.; Hirva, P.; Haukka, M. *J. Chem. Theory Comput.* **2009**, *5*, 1084.
(72) Fowe, E. P.; Therrien, B.; Suss-Fink, G.; Daul, C. *Inorg. Chem.* **2007**, *47*, 42.
(73) Makal, A. M.; Plażuk, D.; Zakrzewski, J.; Misterkiewicz, B.; Woźniak, K. *Inorg. Chem.* **2010**, *49*, 4046.